J.C.M., May 1990, pp.536-558, vol.24.

# STATIC COMPRESSION FAILURE OF CARBON FIBRE T800/924C COMPOSITE PLATE WITH A SINGLE HOLE

C. Soutis and N.A. Fleck
Cambridge University Engineering Department
Trumpington Street, Cambridge CB2 1PZ. Phone 0223 332600

## 1 Summary

This paper describes an experimental and theoretical study of the compressive failure of carbon/epoxy, T800/924C, composite laminates.

Static tests were carried out to investigate the mechanics of uniaxial compressive failure in multidirectional unnotched $[(\pm 45/0_2)_3]_s$ plates. Fibre microbuckling in the 0° plies is the critical damage mode which causes fracture of the composite plate.

A series of experiments was also carried out to determine the failure in compressively loaded $[(\pm 45/0_2)_3]_s$ laminates with circular holes. X-ray radiography and scanning electron microscopy were used to observe damage initiation and propagation. Failure is initiated as matrix cracking. With increasing load fibre microbuckling, surrounded by delamination, occurs at the edges of the hole at locations of high in-plane compressive stress. When damage reached a critical state the laminate failed catastrophically.

Finally, a theoretical model is presented for predicting the static strength of notched laminates. Theoretical predictions are compared with experimental data for specimens containing circular holes of different sizes. Agreement of theory with test data is acceptable.

## 1 Introduction

The response of composite laminates under compressive loading is an important example of the need for established relationships between damage and material properties and is a current problem in structural design. Although it is possible to perform laboratory tests on composite coupons and measure certain response data for a controlled set of loading, geometry and material conditions, the question of how these data relate to the compressive response of structural laminates is, as yet, unresolved.

Frequently, the design of composite structures includes discontinuities such as cutouts and holes. Experimental studies of compression loaded laminates indicate that severe strength reduction can occur due to the presence of these stress raisers [1-3]. It is therefore important to take account of this notch sensitivity both when designing CFRP structural components in which there are joints, bolt holes and cut-outs, and when making allowance for possible manufacturing defects and in-service damage.

This paper describes the types of failure modes encountered in multidirectional carbon/epoxy, T800/924C, composite laminates under compressive loading. It also refers to the influence of a single circular hole on their static compressive strength. The test results are compared with predicted trends using a new failure model based on the stress distribution adjacent to the circular hole and the stress intensity factor, $K_I$, for a crack emanating from the edge of the hole.

## 2 Experimental procedure

The specimens tested in this investigation were fabricated from commercially available carbon/epoxy preimpregnated tapes. The tapes were made of unidirectional Torray 800 carbon fibres preimpregnated with Ciba-Ceigy 924C epoxy resin. The material was laid up by hand in 1m x .3m panels using a $[(\pm 45/0_2)_3]_s$ balanced lay up with the $\pm 45°$ plies on the outside to delay delamination. The $[(\pm 45/0_2)_3]_s$ laminates were moulded to a thickness of about 3.2mm in an autoclave at the Royal Aerospace Establishment (RAE), Farnborough. Following cure, the laminates were ultrasonically

inspected to establish specimen quality and void content. Test material was kept in an ambient laboratory air environment.

Test coupons 245mm long by 50mm wide were cut from the 1m x 0.3m panels, and reinforcement tabs of aluminium alloy were bonded to the carbon fibre reinforced plastic (CFRP) specimens for testing, giving a gauge length of 116mm. Circular holes of various sizes were drilled at the centre of the coupon. The holes were machined using a tungsten carbide bit to minimise fibre damage at the hole boundary. Generally, the drilling procedure produced clean hole surfaces, but some delamination was detected between the first two plies on the drill exit surface of the specimen. Test observations indicated that the delaminations did not play a significant role in the failure process. Foil strain gauges, 2mm long, were placed back-to-back on each side of the coupon far away from the hole to monitor the remote strain. Also small strain gauges, 1mm long, were fixed close to the hole in order to measure local strain, see the insert of figure 2.

Plain specimens without holes were made for measuring the unnotched failure stresses and elastic moduli. Six CFRP coupons of size 245mm x 30mm were cut from the 1m x 0.3m panel and end tabs affixed; strain gauges were glued to each coupon in order to monitor the strain.

An anti-buckling device, similar to that discussed by Curtis [4] was designed to prevent column buckling. Its window size was 90mm long by 38mm wide (20mm for unnotched specimen), based on the decision that local buckling associated with delamination around the holes should not be restrained, but that the specimen should be restrained from general buckling, so that testing can cover the full material strength range. The anti-buckling guides increase the flexural stiffness of the composite plate but carry no load. Teflon tape was used on the inside surfaces of the fixture to reduce friction.

Compressive tests were performed on a screw driven machine (Instron 1195) at a constant rate of crosshead displacement of 1mm/min. The specimens were loaded by shear action using compression wedge grips. The applied torque on the bolt which tightens the grips was 50 Nm; this was adequate to prevent slipping of the specimen

but insufficient to cause end crushing. Considerations of importance throughout the testing procedure were alignment of the coupon in the lower and upper grip and proper attachment of the anti-buckling guides to the specimen.

Most of the specimens with holes were loaded in compression to failure. However, several specimens with 5mm hole diameter were tested by loading the coupon to almost the failure load and then removing the specimen from the test frame. The damage in these coupons was evaluated by using X-ray radiography and scanning electron microscopy (SEM).

## 3 Test Results and Discussion

### 3.1 Unnotched Coupons

Six coupons without holes were tested in compression to determine their failure loads and strains. The stress-strain response of a selected specimen is shown in figure 1. The longitudinal strain on the two faces of the coupon is initially the same but as the applied load is increased the strains diverge indicating bending. The bending cannot be totally avoided in a compression test. It may be the result of an initial imperfection in the specimen. The mean line plotted through the strain points exhibited an initial straight portion with an elastic modulus of 89 GPa, followed by a continuously curved portion with a tangential modulus at failure approximately 11% less than that of the linear part. The theoretical longitudinal modulus for this laminate is 92 GPa. This is calculated using classical laminate plate theory and the basic unidirectional ply elastic constants, table 1. In this table, the $E_L$ modulus of the 0° ply is for compression. The mean failure stress is 810 MPa, with a standard deviation, $s_{n-1}$, of 80 MPa. The average failure strain is 1.10% with an $s_{n-1}$ 0f 0.09%.

The scatter in strength is probably due to imperfect manufacturing conditions of these laminates resulting in fabrication defects and nonuniform laminate thickness. Imperfections in the specimen geometry produces misalignment of the coupon in the testing fixture that causes bending and significant reduction in the measured compres-

sive strength.

Immediately prior to catastrophic fracture distinct cracking sounds are heard. Failure is sudden and 'brittle' like and it occurs within the specimen's gauge length. Fibre microbuckling in the 0° plies is the critical damage mechanism which causes failure of the composite plate. The 0° plies generally fail on a line at either $+15°$ or $-15°$ to the horizontal axis.

## 3.2 Specimens with Single Hole

*Stress-strain data*

All test pieces failed from the hole in a transverse direction to the loading axis at lower loads than for the unnotched coupons. Post-failure examination shows much delamination and fibre microbuckling along the plane of fracture but little damage occurs away from the hole.

The specimens exhibited less than 5% scatter in strength. This implies that the hole controls the fracture strength rather than a defect remote from the hole. The mean gross section failure stress of the specimen with 5mm hole was 430 MPa and the average failure strain 0.55% (average of six tests). It can be seen that the 5mm hole reduced the strength of the laminate by 45%. A plot of the axial stress as a function of the far field axial strain for a selected specimen is shown in figure 2. Strain gauge measurements at the hole edge are included in the figure. The gauges 2 and 3 show higher strain than that of the remote gauge because they are located at the edge of the strain gradient surrounding the hole. After fibre microbuckling occurs ,these gauges read an artificially higher strain because the damage zone grows underneath the gauges. Guynn [5] moved the gauge 3 to a new location just above the damage zone and she found that the local stress supported by the buckled region was lower than the applied compressive stress measured at the control gauge in a remote location.

The axial strain,$\epsilon_{yy}$, measured in the vicinity of the 5mm diameter hole is shown in figure 3, normalised by the remote axial strain, $\epsilon_a$, of 0.25% and is compared with values obtained from 2-D finite element analysis (F.E). The ratio of measured strain to applied

strain given by the gauge inside the hole is 3.4, slightly smaller than the F.E value of 3.48 (the theoretical value is 3.52, Green [6]). The strains near the hole decrease rapidly to the value of the remote strain as the distance from the hole increases. Agreement between F.E results and experiment is good. The general trends are predicted quite well.

In order to study the effect of hole diameter on failure stress, fifteen specimens with a single hole of 6, 7, 8, 10 and 15mm diameter were tested. All specimens failed through the hole at applied loads that decreased as the hole diameter was increased. It can be seen in figure 4 that the experimental data points are bounded by simple criteria based on notch sensitivity, Mikulas [7]. If the material is notch insensitive, the failure stresses are directly proportional to the reduction in cross-sectional area, while if the material is notch sensitive then it is postulated that the material fails when the stress concentration at the hole edge equals the failure stress of the material. The fact that the data points are above the notch sensitive curve indicates that the material is not ideally brittle and some load redistribution does occur around the hole. Examination of the damaged specimens reveals that fibre microbuckling occurs in the vicinity of the hole prior to catastrophic failure. The dotted line in figure 4 is obtained by using the new strength prediction model, described later in this paper.

*X-ray Radiography Results*

The damage in the specimens was evaluated by using penetrant-enhanced X-ray radiography. Zinc iodide has been shown to be an effective penetrant for highlighting damage regions of composites for X-radiography, Scott [8]. Shadow radiographs were taken with the plane of the specimen oriented parallel (face view) to the film, allowing the X-ray beam to travel through the thickness. The radiographs were enlarged and printed on high-contrast printing paper to accentuate damage detail.

Typical penetrant enhanced X-ray photographs of static loading induced damage are shown in figures 5 and 6. The damage consists of matrix cracks parallel to the fibres, delamination between the layers and fibre microbuckling. Delaminations appear as dark shaded regions and the matrix cracks are superimposed through the thickness

in the flat radiographs, appearing as a single, thick crack.

Consider first figure 5, for which the applied load is 80% of the failure load. Prior to loading, machining damage existed in the form of delamination between the outer $+45°$ and $-45°$ laminae. This damage is marked 'A' in figure 5. On loading to 75% of the ultimate strength tensile cracking occurs between the $0°$ fibres at the top and bottom of the hole, marked 'B' in figure 5.

Now consider figure 6, which shows the same specimen under an applied load of 90% of the failure load. The delaminated region 'A' is identical in extent to that of figure 5. The $0°$ splits marked 'B' have grown from an average length of $1.5mm$ in figure 5 to an average length of $2mm$ in figure 6 and have increased in density. Additional splits develop in the $0°$ plies tangentially to the hole, marked 'C' in figure 6. In the $0°$ central plies these splits are generally asymmetric and this is probably related to the centre ply asymmetry; *i.e.* $0°$ plies at mid-plane are adjacent to a $-45°$ ply on both sides. Many short $-45°$ tensile cracks exist along the path of the $0°$ splits and are marked as 'D' in figure 6.

The finite element analysis predicts that the matrix in the $0°$ laminae fails essentially by shear. At 90% of the failure load the shear stress along the path of the $0°$ splits is of similar magnitude to the shear strength of a unidirectional lamina. This shear failure is associated with protrusion of the $0°$ fibres into the hole, and causes tensile splitting of the $-45°$ plies, feature 'D' of figure 6. Subsequent examination by the deply technique revealed that the $-45°$ plies adjacent to the central $0°$ layers underwent bending failure.

Fibre microbuckling, surrounded by delamination, develops at the edges of the hole at areas of high in-plane compressive stress. This local buckling on an X-ray radiograph resembles a crack and is marked 'E' in fig. 6. As the remote load is increased further the crack extends. At maximum load the microbuckled zone propagates rapidly and the laminate breaks. The final fracture surface is transverse to the loading axis.

*Scanning Electron Microscope Results*

The location and nature of damage in individual plies was obtained by using the deply technique, Freeman [9]. The damaged surfaces produced by peeling were examined in the scanning electron microscope (SEM).

At low load level, no damage is evident either on the faces or in the bore of the hole. As the load is increased up to 70-75% of the failure load the first sign of damage is protrusion of the discontinuous 0° fibres into the bore of the hole. This fibre movement induces some delamination and matrix splitting in the axial plies. The damage becomes more pronounced at about 90-95% of the specimen's ultimate strength, fig. 7. Figure 7, reveals that fibre microbuckling occurs first in the 0° plies closest to the surface accompanied by delamination in the 45/0-ply interface. It is clear that fibre microbuckling is confined to areas subjected to high axial compressive stress.

SEM photographs illustrating damage in different plies are shown in figures 8 and 9. Matrix cracking in the axial plies is associated with failure in adjacent off-axis plies, figure 8. The long vertical splits tangent to the hole in the 0° plies at the mid-plane of the laminate, are accommodated in the adjacent $-45°$ plies by slight kinking of the individual fibres. In figure 9, the fibre microbuckling in a 0° ply appears to have originated from a point where a 0° split terminates. Its direction is initially governed by a short matrix crack parallel to the fibres in the adjacent $+45°$ ply, but further away from the hole the fracture line becomes almost perpendicular to the loading axis. Very few 45° cracks are observed in the off-axis plies, to influence the failure mode. Failure of the composite laminate occurs as a result of fibre buckling in the axial plies. The failure of the 0° fibres is mainly due to the high axial compressive load. It is probable that fibre/matrix debonding and matrix yielding help fibre buckling by reducing the side support for the fibres.

## 4 Fracture Mechanics Concepts

For isotropic materials the subject of linear elastic fracture mechanics (LEFM) is highly developed and the plane strain fracture toughness, $K_C$, is treated as a material property. Paris and Sih [10] developed expressions for the crack tip stress field for a linear elastic anisotropic material for the case of plane strain and pure shear. The crack tip stress field exhibits the same $r^{-\frac{1}{2}}$ singularity with distance $r$ from the crack tip as for the isotropic case. Also the stress intensity factors, (SIF), $K_I$, $K_{II}$, $K_{III}$ have the same meaning as for the isotropic case.

Linear elastic fracture mechanics can be applied to composite laminates provided the damage zone at the crack tip is contained within the K-field, *i.e.* provided the damage zone is small compared with other dimensions of the specimen.

In this section the fracture toughness $K_C$ of the T800/924C laminate is reported based on a finite element calibration of the stress intensity factor for a centre-cracked plate.

### 4.1 Stress Intensity Factors for Centre-Cracked Specimens

The stress intensity factor for a finite two dimensional isotropic plate, subjected to mode I loading and containing a single straight crack of length 2a, figure 10, is given by

$$K_I = \sigma^{\infty}\sqrt{\pi a}\, f(a/W) \tag{4.1}$$

where $\sigma^{\infty}$ is the applied far field stress and the factor $f(a/W)$ reflects the influence of geometry on the SIF. Numerical values of the $f(a/W)$ factors have been obtained using numerical and experimental techniques for a number of typical fracture test configurations, for example Isida [11], Koiter[12].

The K-calibration factor $f(a/W)$ also depends upon material anisotropy. Using finite element analysis $K_I$ for an orthotropic T800/924C centre-cracked composite plate

is now determined.

## 4.2 Description of the Finite Element Analysis (FEA)

Over the last decade or so, the finite element method, (FEM), has become firmly established as a standard procedure for deriving values of SIF. A number of techniques is currently used for evaluating SIFs. Here the virtual crack extension procedure in the MARC finite element package, with the 1/4 point crack tip element is used to obtain the SIF for a centre-cracked tensile specimen.

*Quarter Point Elements*

The fundamental difficulty in a crack problem is the singularity in the strain field at the crack tip. The singularity in the strain field is of the order $r^{-\frac{1}{2}}$, where $r$ is the distance from the crack tip. The finite element mesh must be such that the singularity is approximated with sufficient accuracy. Many methods have been devised to arrive at such an approximation; however, the most commonly used method uses a degenerated form of the standard 8-node quadrilateral element. This isoparametric element produces the $r^{-\frac{1}{2}}$ singularity when it degenerates to a triangular element and the mid-side nodes are moved to the quarter point adjacent to the crack tip node.

*J-Integral Evaluation*

The MARC program allows the evaluation of the J-integral by moving nodes within a certain ring of elements around the crack tip, to represent a differential crack advance, $\delta l$, and measuring the change in strain energy, $\delta U$. The J-integral is the negative differential of strain energy with respect to crack advance. For an elastic body $J$ is identical to the elastic strain energy release rate $G$. Hence,

$$G = J = -\frac{\partial U}{\partial l} \tag{4.2}$$

The finite element mesh in figure 11 has three "rings" of elements around the crack tip (not shown), so that three evaluations of $J$ are available. Since the $J$-integral should be path independent for elastic problems, the variation in $J$ between the three

values gives a measure of the accuracy of the solution. A crack extension, $\delta l$, has to be supplied to evaluate $J$ and its value must be less than 1/50 times the size of the smallest crack tip element. A rather coarse mesh is needed, because the only output required is the $J$-integral value, and Parks [13] has shown that the differential stiffness technique, as used in MARC, provides good estimates of $J$ with relatively coarse meshes.

### 4.3 Relationship between K and G

For an orthotropic laminate the energy release rate $G$ is related to the stress intensity factor $K_I$ by

$$G_I = cK_I^2 \tag{4.3}$$

where for plane stress loading, $c$ is given by Paris, *et.al* [10]

$$c = \left(\frac{a_{11}a_{22}}{2}\right)^{\frac{1}{2}} \left[\left(\frac{a_{22}}{a_{11}}\right)^{\frac{1}{2}} + \frac{2a_{12}+a_{66}}{2a_{11}}\right]^{\frac{1}{2}} \tag{4.4}$$

Here, the components of $[a]$ are related to the laminate constants by

$$[a] = \begin{pmatrix} \frac{1}{E_{xx}} & \frac{-\nu_{yx}}{E_{yy}} & 0 \\ \frac{-\nu_{xy}}{E_{xx}} & \frac{1}{E_{yy}} & 0 \\ 0 & 0 & \frac{1}{\mu_{xy}} \end{pmatrix} \tag{4.5}$$

In equation (4.5) $E$ and $\mu$ are the laminate extensional and shear moduli respectively, and $\nu$ is the Poisson's ratio in the reference system shown in figure 10.

## 4.4 Results of SIF Calculations

In order to investigate the accuracy of the finite element model an isotropic stress analysis is performed. The plane strain SIF for a centre-cracked tensile (CCT) specimen, with $a/W = 0.5$, is shown in table 2 and is compared to the value given by Isida [11]. It is clear from these results that the path independence of $J$ is well reproduced, and that the error in the solution for $K_I$ is small.

The values of the K-calibration factor $f(a/W)$ for the CCT orthotropic T800/924C, $[(\pm 45/0_2)_3]_s$, laminate with $L/W = 2.0$ and for crack length varying from 10 to 80% of the specimen width are given in table 3. The factor $f(a/W)$ is a function of both material properties and specimen configuration. The anisotropic SIF is about 2% higher than its isotropic counterpart.

We conclude that the anisotropic effect is small and the isotropic SIF may be employed as an estimate of the anisotropic value.

## 4.5 Fracture Toughness of the $[(\pm 45/0_2)_3]_s$ Laminate

A series of tests was performed on centre-cracked compression specimens to calculate the fracture toughness, $K_C$, of the T800/924C laminate. The crack length-to-width ratios, $a/W$, ranged from 0.2 to 0.8. The toughness values are computed by using the compressive failure stress and the orthotropic K-calibration factors obtained from the finite element analysis. The results are summarised in table 4.

It is apparent that the fracture toughness, $K_C$, is independent of crack size. The experimental value of $46.5 MPa\sqrt{m}$ (or $1470 MPa\sqrt{mm}$) falls within the range of toughness values reported in the literature for $[\pm 45/0]_n s$ graphite/epoxy laminates, Harris *et. al* [14].

## 5 Failure Criteria for Notched Composite Laminates

During the last fifteen years numerous investigations have been conducted in which composite laminate fracture toughness or fracture strength were measured, modes of failure observed and various models used to predict tensile fracture. The main models are summarised here as background to the new theoretical model for predicting the notched compressive strength of composite laminates.

Waddoups [15] postulated the existence of a "high intensity energy region", adjacent to a circular hole on a composite plate under uniaxial tensile load. The "high intensity energy region" behaves like a crack of length $a$. The fracture strength of the composite laminate was taken from $K_{IC}$ and $a$, given the geometry and stress intensity factor. Waddoups made use of the Bowie's [16] solution for the SIF, for the problem of cracks emanating from a circular hole for an isotropic homogeneous infinite plate. This approach of characterising the damage zone using the LEFM stress intensity factor is known as the inherent flaw model, (IFM).

Whitney and Nuismer [17] were able to predict variation of tensile strength with respect to a hole or a straight crack size without recourse to fracture mechanics. They introduced a characteristic length by assuming that fracture depends on attaining a critical stress $\sigma_o$ at a characteristic distance, $d_o$, ahead of the cut-out (Point Stress Failure Criterion, PSFC), or attaining critical average stress $\sigma_o$ along a characteristic distance, $a_o$, ahead of the notch (Average Stress Failure Criterion, ASFC). The characteristic distance is used as a free parameter to be fixed by best fitting the experimental data.

The PSFC and the ASFC have been extended to include compression loaded laminates, Mikulas *et.al* [18] and Nuismer *et.al* [19] respectively. They reported good agreement between experimental and predicted results.

## 5.1 New Failure Prediction Model

In the current experimental work it is observed that at low compressive loads the T800/924C, $[(\pm 45/0_2)_3]_s$ composite notched laminate deforms elastically with no damage. The maximum stress near the hole is not high enough to cause damage. When the applied load increases so that the local stress at the stress raiser reaches a certain value damage occurs in the form of fibre microbuckling, perpendicular to the loading axis. On an X-ray radiograph this failure mode resembles a crack. The microbuckle propagates in the transverse direction under increasing load; at a critical stress level it grows rapidly and catastrophic failure occurs.

Here it is attempted to model the damage initiation and propagation processes using the stress distribution at the edge of the hole and linear fracture mechanics. Microbuckling occurs first as a stable process under increasing load, followed by unstable propagation at maximum load.

### 5.1.1 Fracture Criteria

*i) Stable Crack Growth*

Prediction of stable crack growth is based on a critical stress value and the stress distribution adjacent to the circular hole. It is postulated that microbuckling occurs over a distance $l_b$ from the discontinuity when the average stress over the distance $l_b$ reaches the critical stress of the unnotched laminate, $\sigma_o$, figure 12a.

$$\sigma_o = \frac{1}{l_b} \int_R^{R+l_b} \sigma_{yy}(x,0)dx \tag{5.1}$$

Substituting for $\sigma_{yy}(x,0)$, from equation (A.1) in the appendix, gives:

$$\sigma_o = \frac{\sigma^\infty}{l_b} \int_R^{R+l_b} [A + Bx(x^2 + DR^2)^{-\frac{1}{2}} + Cx(x^2 + ER^2)^{-\frac{1}{2}}]dx \tag{5.2}$$

where

$$\left.\begin{aligned} A &= \frac{(1+\gamma_1)(1+\gamma_2)}{4\gamma_1\gamma_2} \\ B &= \frac{(1+\gamma_2)(1-\gamma_1)^2}{4\gamma_1(\gamma_1-\gamma_2)} \\ C &= \frac{(1+\gamma_1)(1-\gamma_2)^2}{4\gamma_2(\gamma_1-\gamma_2)} \\ D &= \frac{4\gamma_1}{(1-\gamma_1)^2} \\ E &= \frac{4\gamma_2}{(1-\gamma_2)^2} \end{aligned}\right\} \tag{5.3}$$

Equation (5.2) may be integrated to give the stress, $\sigma^\infty$, at which microbuckling occurs, *i.e*

$$\sigma^\infty = \sigma_o\left[\frac{1-\xi}{A+B\sqrt{1+D\xi^2}+C\sqrt{1+E\xi^2}}\right] \tag{5.4}$$

where

$$\xi = \frac{1}{1+l_b/R} \tag{5.5}$$

Microbuckling begins when $l_b = 0$, at a stress $\sigma_i^\infty$ given by equation (5.4).

*(ii) Unstable Crack Growth*

We assume that a microbuckle behaves as a crack of the same length, with no traction on the crack surfaces. The stress intensity factor at the tip of a microbuckle of length $l_b$ from the hole edge, figure 12b, is expressed as

$$K_I = \sigma^\infty\sqrt{\pi l_b}\, f(l/R) \tag{5.6}$$

The length $l_b$ is small but finite. $R$ is the hole radius and $\sigma^\infty$ is the remote applied stress. The correction factor $f(l_b/R)$ is taken from the Bowie [16] analysis for symmetrical cracks emanating from a circular hole in an isotropic material. The values of the $f(l_b/R)$ factors are presented in table 5. The anisotropic effect for the present specimen geometry and material properties given in table 1 is small and it can be neglected.

We assume unstable crack growth occurs when $K_I$ at the tip of the buckled region is equal to the material fracture toughness $K_C$.

## 5.2 Applications

Some examples are presented in this section, which illustrate the application of the new fracture model to composite materials.

Having obtained the unnotched compressive strength, $\sigma_o$, and the fracture toughness $K_C$ of the laminate, the notched compressive failure strength, $\sigma_n$, for any hole radius $R$ can be predicted. The measured values of $\sigma_o$ and $K_C$ are 810 MPa and $46.5MPa\sqrt{m}$ respectively. The general procedure is to plot the ratio of $\sigma^\infty/\sigma_o$, given by equations (5.4) and (5.6), versus $l_b/R$. Then the failure strength, $\sigma_n$, can be obtained from the point where the two curves intersect, figure 13. This point also provides the critical buckled length $l_c$.

Measured and predicted values of notch strength are given in figure 4 as a function of hole size. The agreement is acceptable.

The new model can predict qualitatively the load-damage size relationship for notched composite laminates. The curve in figure 13 shows the progressive growth of the fibre microbuckling zone from initiation to failure for a plate containing a $5mm$ hole. The theoretical strength value is $410MPa$ and is in good agreement with the experimental one of $\sim 430MPa$. The predicted value of stress for initiating microbuckling, $\sigma_i$, is consistently less than the measured value.

Further development of the present model is needed. The redistribution of stresses and decrease of stiffnesses due to damage zone must be taken into account for better agreement between theory and experiment.

## 6 Concluding Discussion

The main failure mechanism observed is fibre microbuckling in the 0° plies. Fibre buckling initiates at the edges of the hole at very high compressive loads (about 90% of the fracture strength). Because of their greater axial stiffness the 0° plies carry most of the load and hence it is the failure of these laminae which results in laminate fracture. Matrix splitting and delamination occur with the microbuckling but are thought to be secondary modes of damage.

A new failure model based on the stress distribution around the notch and the stress intensity factor, $K_I$, is used to predict the notched compressive strength of the multidirectional, $[(\pm 45/0_2)_3]_s$, T800/924C composite laminate with a circular hole. The $K$ approach is justified as the microbuckled zone resembles a crack and damage ahead of the microbuckle is small in extent compared with other specimen dimensions. Correlation of theory with test data is good.

Finally further work is needed to predict more accurately the load-damage size relationship.

ACKNOWLEDGEMENTS

This work was carried out with the financial support of the Procurement Executive of the Ministry of Defence and the Science and Engineering Research Counsil (SERC). The authors would like to express their appreciation to Dr P. Curtis, from the Royal Aerospace Establishment, Farnborough, and to Dr P.A. Smith from Surrey University, for helpful discussions.

## 7 References


1 . STARNES, J.H., RHODES, M.D. and WILLIAMS, J.G. "Effect of Impact and Holes on the Compressive Strength of a Graphite/Epoxy Laminate", ASTM STP 696, pp 145-171.

2 . GARBO, S.P. "Compression Strength of Laminates with Unloaded Fastener Holes", MCAIR-80-005, May 1980.

3 . POTTER, R.T. "The Environmental Degradation of Notched CFRP in Compression". Composites, Vol.14, No3, July 1983.

4 . CURTIS, P.T. "CRAG Test Methods for the Measurement of the Engineering Properties of CFRP", RAE TR-85099, 1985.

5 . GUYNN, E.G. and BRADLEY, W.L. "Micromechanics of Compression Failures in Open Hole Composite Laminates", ASTM STP 1012, P.A. Lagace, ed., 1989.

6 . GREEN, A.E. Proceedings of the Royal Society of London, Vol.180A, p173, 1942.

7 . MIKULAS, M.M "Failure Prediction Techniques for Compression Loaded Composite Laminates with Holes", NASA CP 2142, Aug.1980.

8 . SCOTT, I.G. and SCALA, C.M. "A Review of Non-destructive Testing of Composite Materials", NDT International, April 1982.

9 . FREEMAN, S.M. "Characterization of Lamina and Interlaminar Damage in Graphite/Epoxy by the Deply Technique", ASTM STP 787, pp 50-62, 1982.

1 0. PARIS, P.C. and SIH, G.C. "Stress Analysis of Cracks. Fracture Toughness Testing and its Applications", ASTM STP 381, pp 30-83, 1965.

1 1. ISIDA, M "Analysis of SIF for the Tension of a Centrally Cracked Strip with Stiffened end", Eng. Fracture Mech., 1973.

1 2. KOITER, W.T. "Note on the SIF for Sheet Strips with Cracks under Tensile Load. Univ. of Technology, Lab. of Engineering Mechanics, Report No 314, Delft, Netherland, 1965.

1 3. PARKS,D.A. "Fracture Behaviour of Thick, Laminated Technique for Determination of Elastic Crack Tip SIF", Int. J. Fracture. Vol.10, No 4, pp 487-502, 1974.

1 4. HARRIS, C.E. and MORRIS, D.H. "Fracture Behaviour of Thick, Laminated Graphite/Epoxy Composites", NASA Contractor Report 3784, 1984.

1 5. WADDOUPS, M.E., EISENMAN, J.R. and KAMINSKI, B.E. "Macroscopic Fracture Mechanics of Advanced Composite Materials", J.Comp. Materials, Vol.5, pp 446-454, 1971.

1 6. BOWIE'S, O.L. "Analysis of an Infinite Plate Containing Radial Cracks Originating from the Boundary of an Internal Circular Hole", J. Math and Physics, Vol.35, pp 60-71, 1956.

1 7. WHITNEY, J.M. and NUISMER, R.J. "Stress Fracture Criteria for Laminated Composites Containing Stress Concentrations", J. Comp. Mater., Vol.8, pp 253-265, 1974.

1 8. MIKULAS, M.M., RHODES,M.D. and McGOWAN, P.E. "Effects of Orthotropy and Width on the Compression Strength of Graphite/Epoxy Panels with Holes", AIAA journal, Vol.22, No.9, pp 1283-1292, 1984.

1 9. NUISMER, R.J. and LABOR, J.D. "Applications of the Average Stress Failure Criterion : Part II-Compression", J. Composite Materials, Vol.13, pp 49-60, 1979.

2 0. SMITH, P.A. "Behaviour of Bolted Joints in $(0/90)_{ns}$ Laminates", CUED/C-Mat/TR121, Cambridge University, England, 1985.

# 1 Appendix

## 1.1 Stress Concentrations for Orthotropic Plates with Holes

Following the work of Green [6], Smith [20] expressed the stress distribution along the $y = 0$ in an infinite orthotropic plate containing a hole of radius $R$, under remote uniaxial stress, $\sigma^{\infty}$, as:

$$\sigma_y = \sigma^{\infty}[\frac{(1+\gamma_1)(1+\gamma_2)}{4\gamma_1\gamma_2} + \frac{1}{4(\gamma_1-\gamma_2)}\left\{\frac{(1+\gamma_2)(1+\gamma_1)^2}{\gamma_1 X_1} - \frac{(1+\gamma_1)(1-\gamma_2)^2}{\gamma_2 X_2}\right\}] \tag{A.1}$$

where

$$\left.\begin{aligned} X_1 &= \sqrt{\frac{(x/R)^2(1-\gamma_1)^2+4\gamma_1}{(x/R)^2(1-\gamma_1)^2}} \\ X_2 &= \sqrt{\frac{(x/R)^2(1-\gamma_2)^2+4\gamma_2}{(x/R)^2(1-\gamma_2)^2}} \end{aligned}\right\} \tag{A.2}$$

The terms $\gamma_1$ and $\gamma_2$ are related to the laminate's moduli via constants $\alpha_1$ and $\alpha_2$:

$$\left.\begin{aligned} \gamma_1 &= \frac{\sqrt{\alpha_1}-1}{\sqrt{\alpha_1}+1} \\ \gamma_2 &= \frac{\sqrt{\alpha_2}-1}{\sqrt{\alpha_2}+1} \end{aligned}\right\} \tag{A.3}$$

where

$$\left.\begin{aligned} \alpha_1\alpha_2 &= \frac{E_{xx}}{E_{yy}} \\ \alpha_1+\alpha_2 &= (\frac{1}{G_{yx}} - \frac{2\nu_{yx}}{E_{yy}})E_{xx} \end{aligned}\right\} \tag{A.4}$$

In figure 3, the ratio $\sigma_y/\sigma^{\infty}$ is plotted versus $x/R$ from the finite element solution for a finite plate of hole radius-to-width ratio, $R/W = 0.1$. The analytic solution (A.1) for an infinite plate is included. The two solutions are identical for practical purposes.

Table 1

Laminate Stiffness Properties

| Property/GPa | $0^\circ$ | $[(\pm 45/0_2)_3]_s$ |
|---|---|---|
| $E_L$ | 161 | 92 |
| $E_T$ | 9.25 | 25.8 |
| $\upsilon_{LT}$ | 0.34 | 0.69 |
| $G_{LT}$ | 6.0 | 23.6 |

Table 2

K - Calibration Factor for Isotropic plate (a/w = 0.5)

Isida found $K_I = 1.1867\sigma^{\infty}\sqrt{\pi a}$

| Variable | move tip only | move 1st ring of elements | move 2nd ring |
|---|---|---|---|
| $\frac{K_I}{\sigma^{\infty}\sqrt{\pi a}}$ | 1.2034 | 1.20125 | 1.2007 |
| Error | 1.387% | 1.2112% | 1.16% |

Table 3

K - Calibration Factors for Plate with L/W = 2.0, $E_T/E_L \approx 0.3$

| a/w | $f(a/w)_{ISIDA}$ | $f(a/w)_{ORTH}$ |
|---|---|---|
| 0.1 | 1.006 | 1.0181 |
| 0.2 | 1.0246 | 1.0382 |
| 0.3 | 1.0577 | 1.0786 |
| 0.4 | 1.1094 | 1.1289 |
| 0.5 | 1.1867 | 1.2114 |
| 0.6 | 1.3033 | 1.3205 |
| 0.7 | 1.4882 | 1.5120 |
| 0.8 | 1.816 | 1.8145 |

Table 4

Fracture Toughness of the T800/924C $[(\pm 45/0_2)_3]_s$ Laminate, L/W = 2.0, $E_T/E_L \approx 3$

| a/mm | a/w | $\sigma_F$/MPa | $K_{Ic}$/MPa $\sqrt{m}$ |
|---|---|---|---|
| 5 | 0.2 | 346 | 45.02 |
| 10 | 0.4 | 239 | 47.82 |
| 15 | 0.6 | 163 | 46.72 |
| 20 | 0.8 | 102 | 46.39 |

$^* K_{IC}^{mean} = 46.5$ MPa $\sqrt{m}$

Table 5

f($\ell$/R) Factors for an Infinite Plate with Cracks Emanating from a Hole

| $\ell$/R | 0.1 | 0.2 | 0.3 | 0.4 | 0.5 | 0.6 | 0.8 | 1.0 |
|---|---|---|---|---|---|---|---|---|
| f($\ell$/R) | 2.73 | 2.41 | 2.15 | 1.96 | 1.83 | 1.71 | 1.58 | 1.45 |

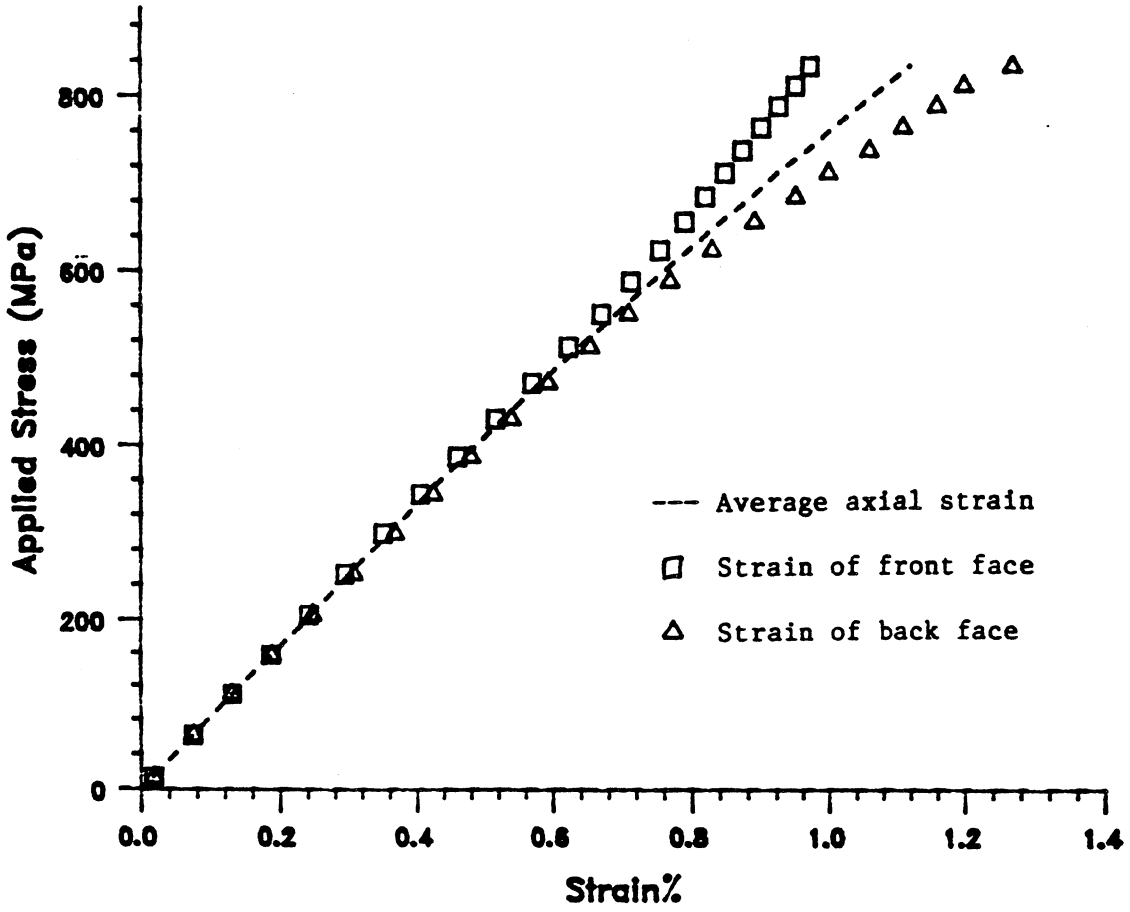


Fig.1. Compressive stress-strain response of multi-directional T800/924C composite laminate, unnotched specimen.

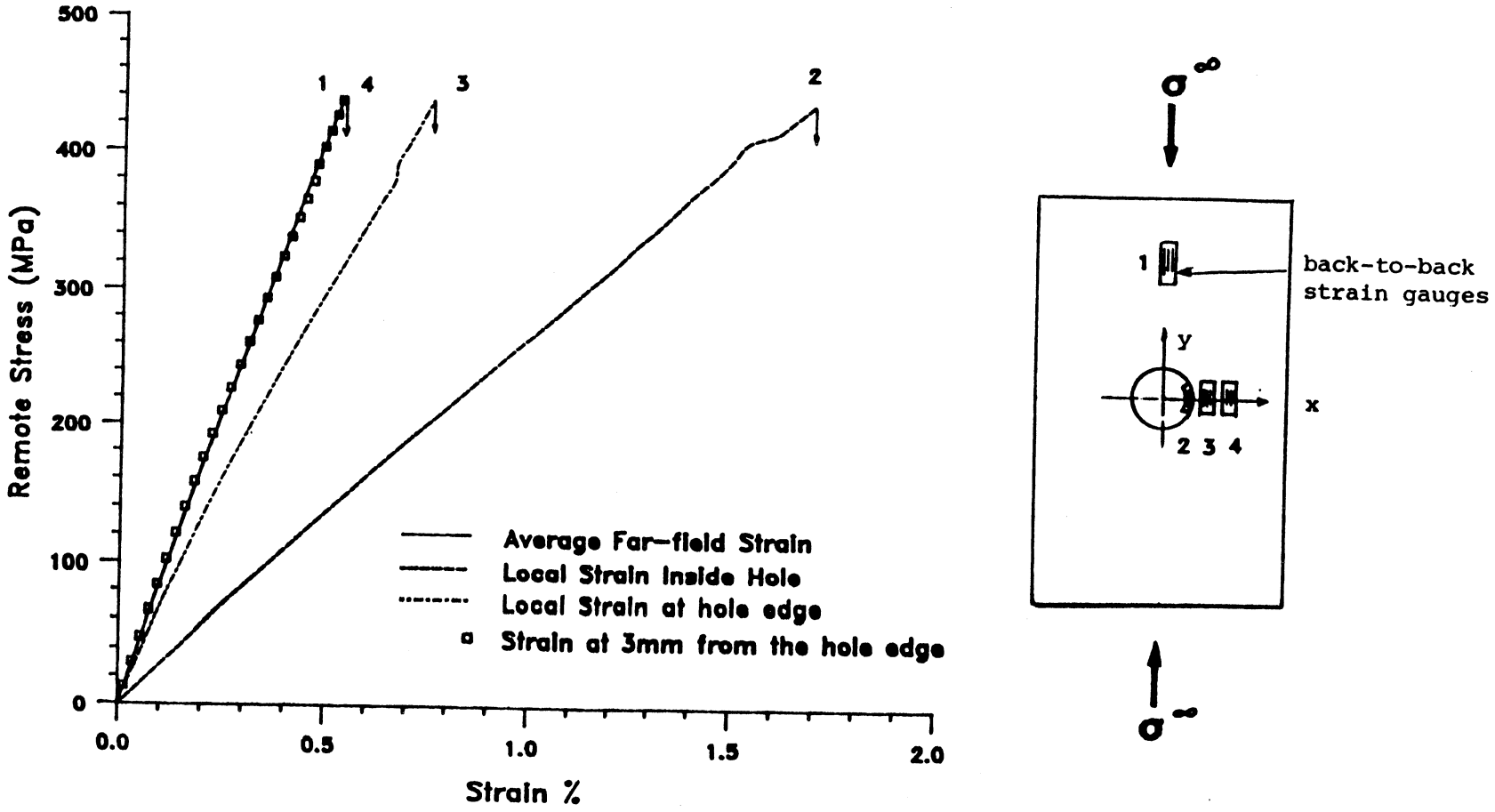


Fig.2. Stress-strain response of notched multi-directional specimen (d=5mm).

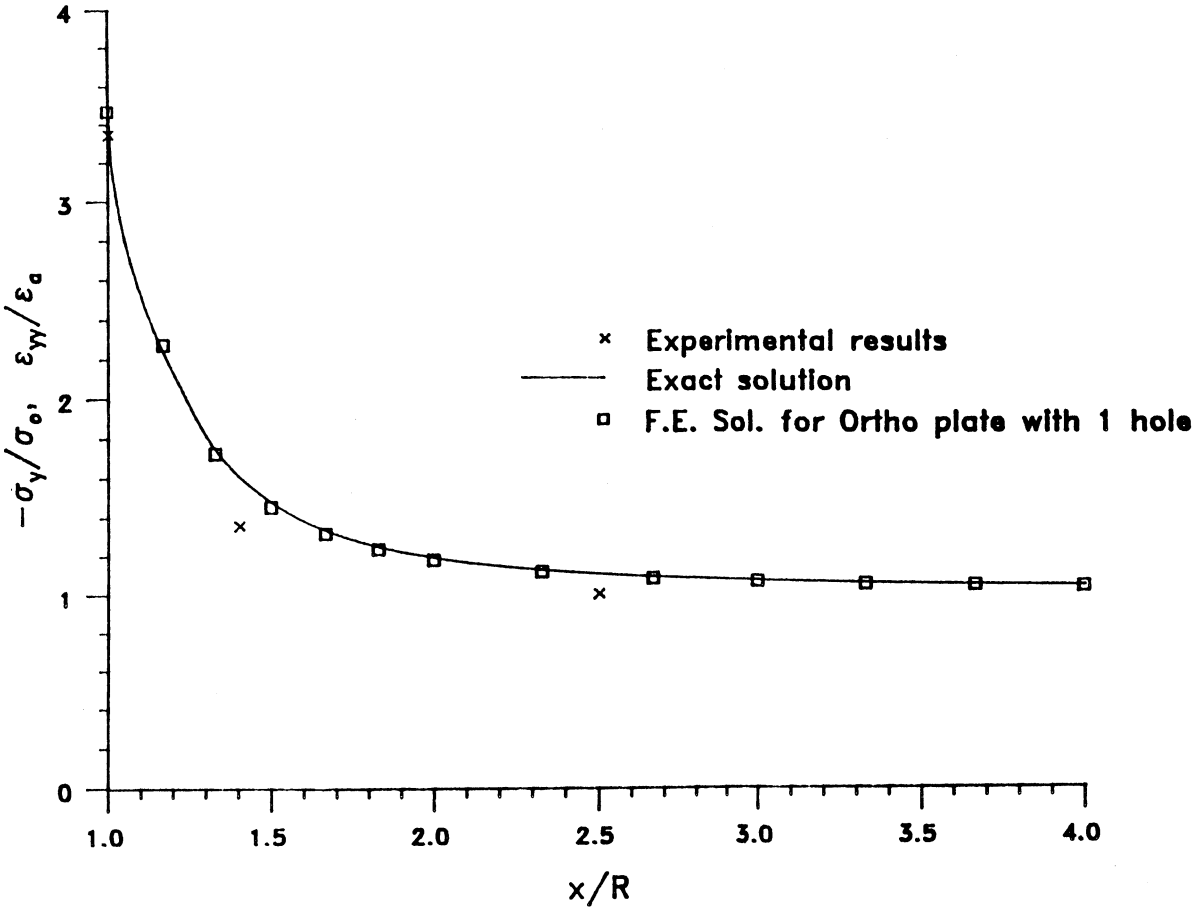


Fig.3. Normal stress (strain) distribution of a T800/924C orthotropic plate with a single hole (d/W=0.1).

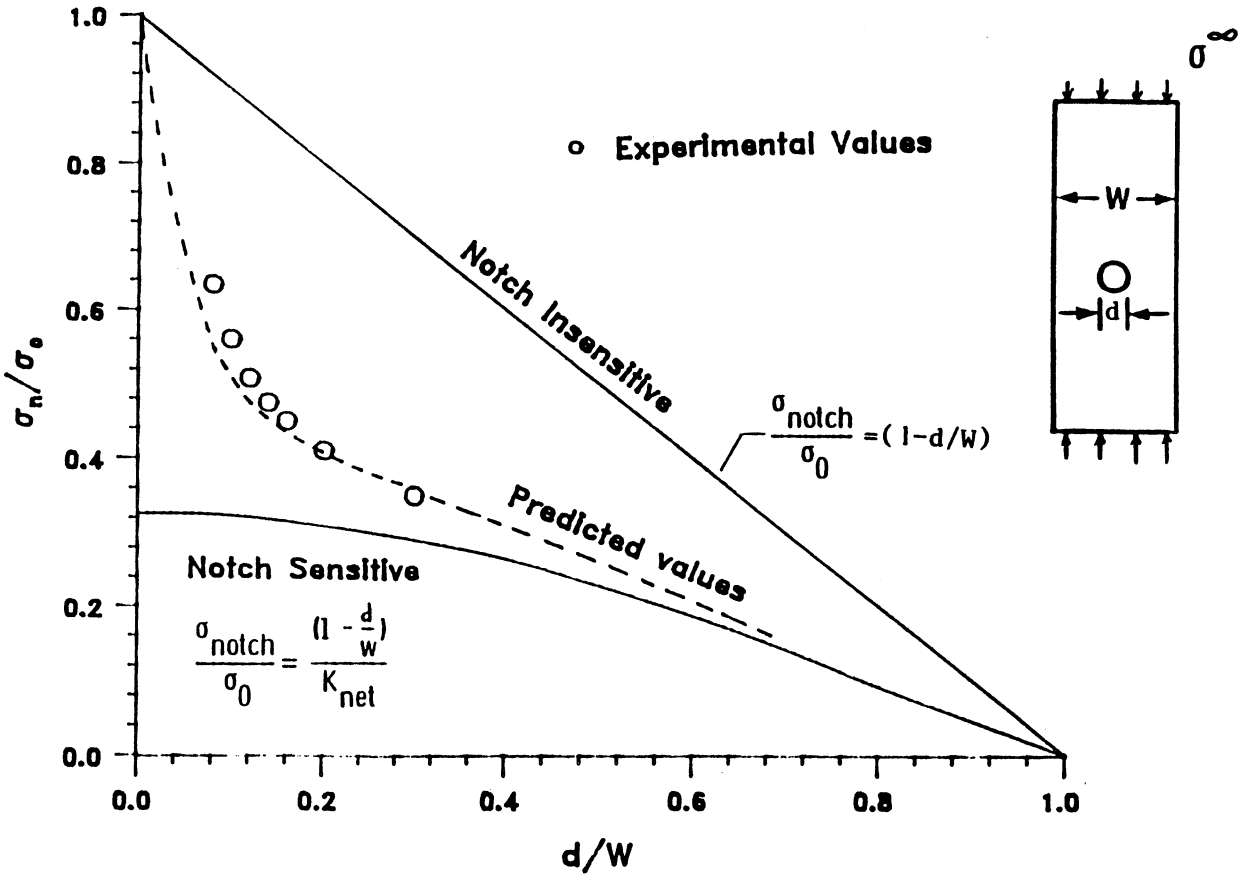


Fig.4. Effect of hole diameter on the strength of a T800/924 orthotropic composite plate.

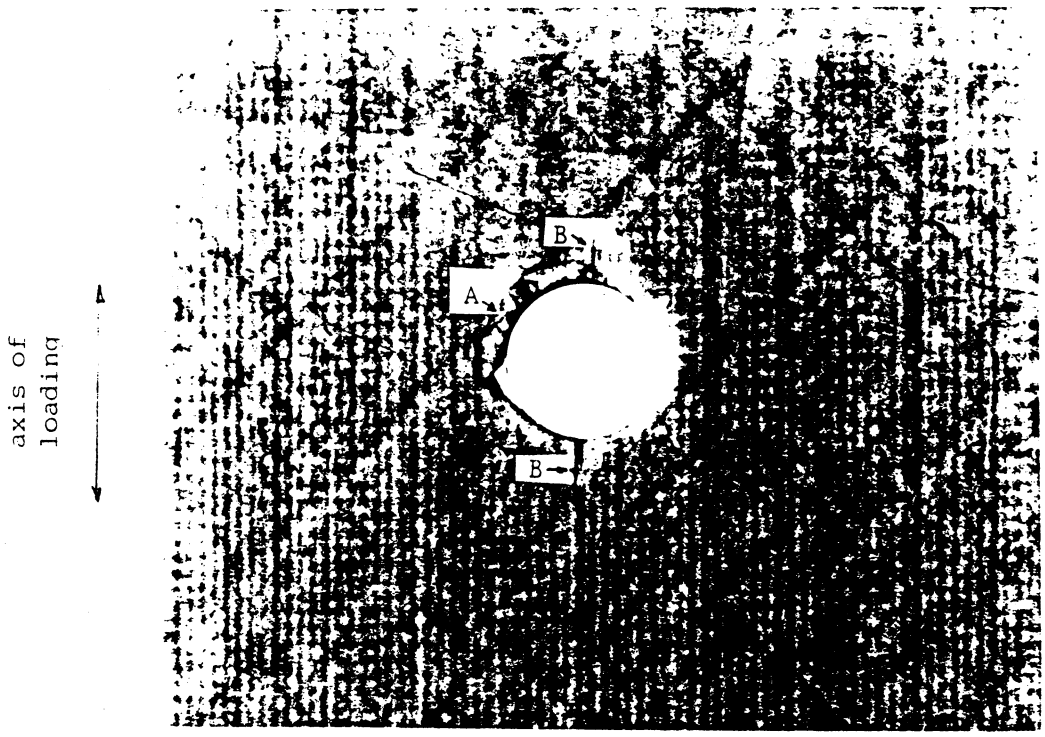


Fig.5. X-ray radiograph taken at 80-85% of laminate's failure load. Some matrix cracking occured on top of the hole. The delamination is mainly due to drilling damage. Applied strain 0.45%.

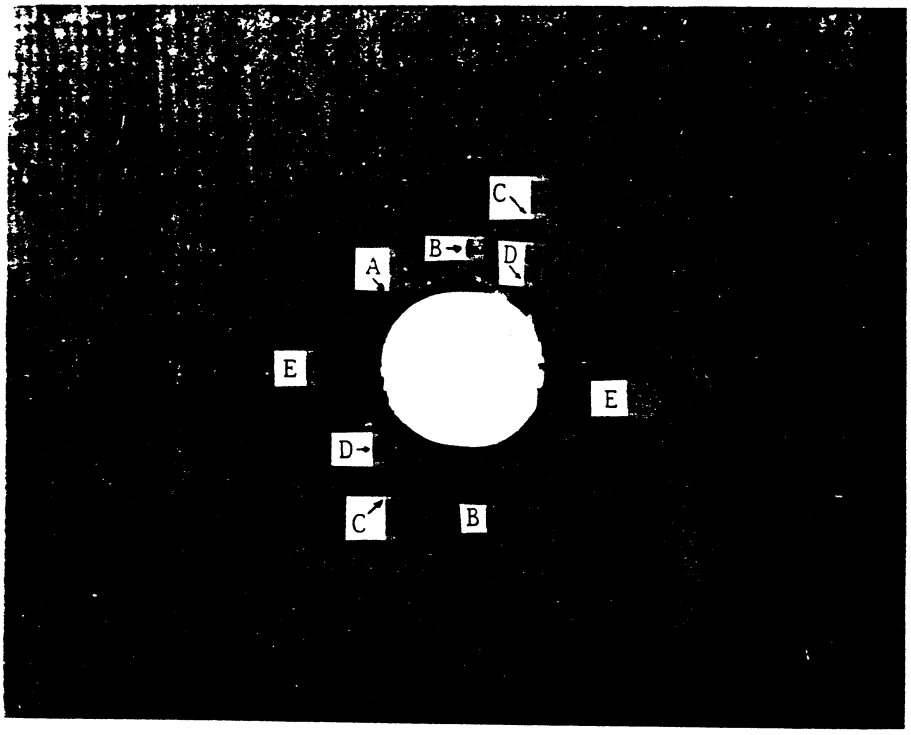


Fig.6. Damage at 90-95% of failure load. It consists of long cracks tangent to the hole and fibre microbuckling surrounded by delamination. Appl. strain 0.504%.

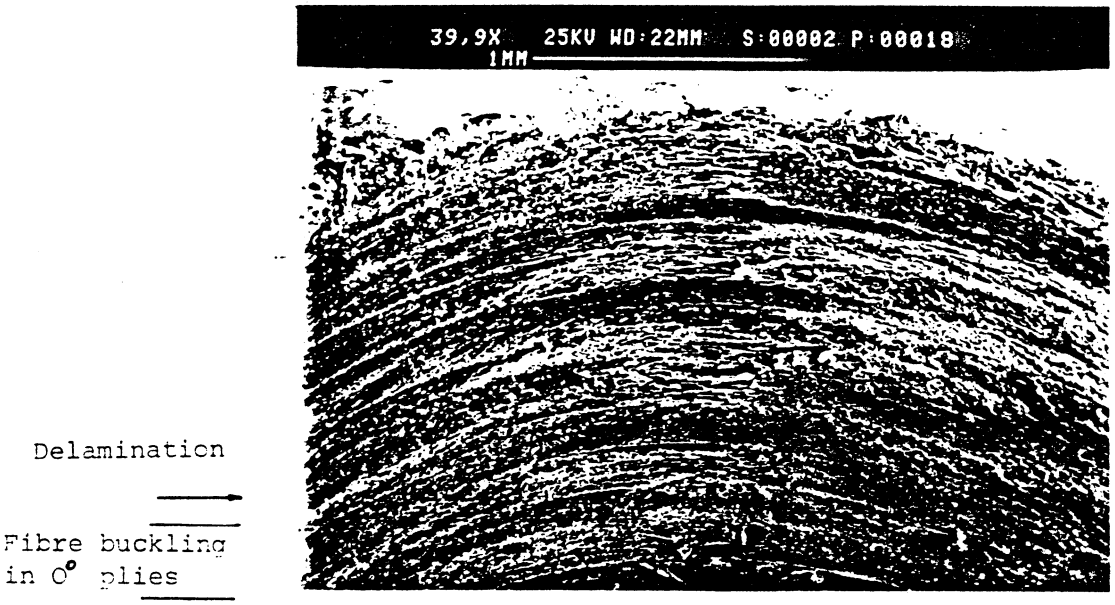


Fig.7. a) Damage into the bore of the hole at 90-95% of ultimate strength. Applied strain 0.504%. 0-deg plies close to the surface show fibre microbuckling failure.

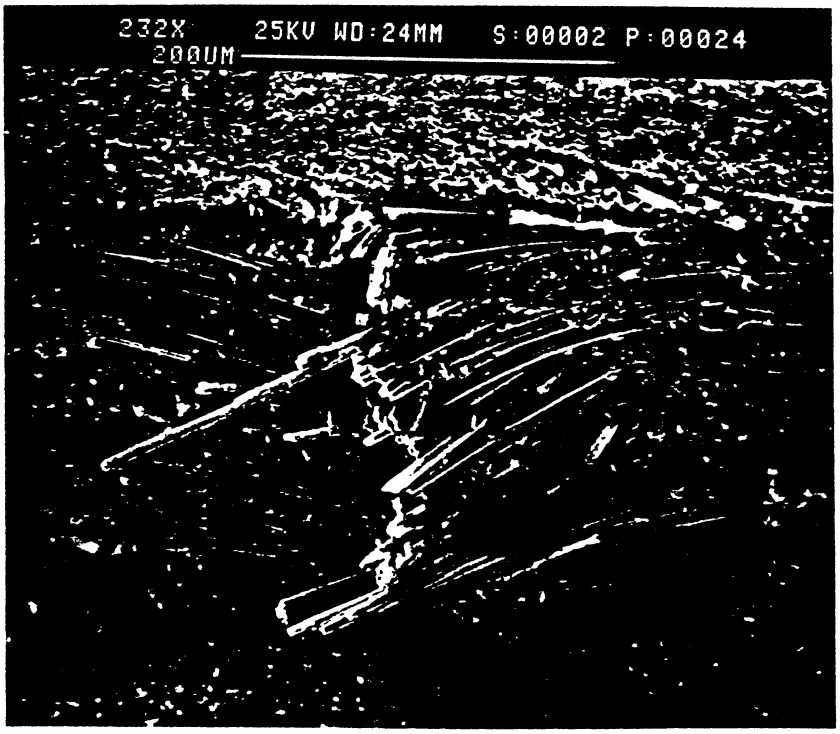


b) Close-up view of (a).

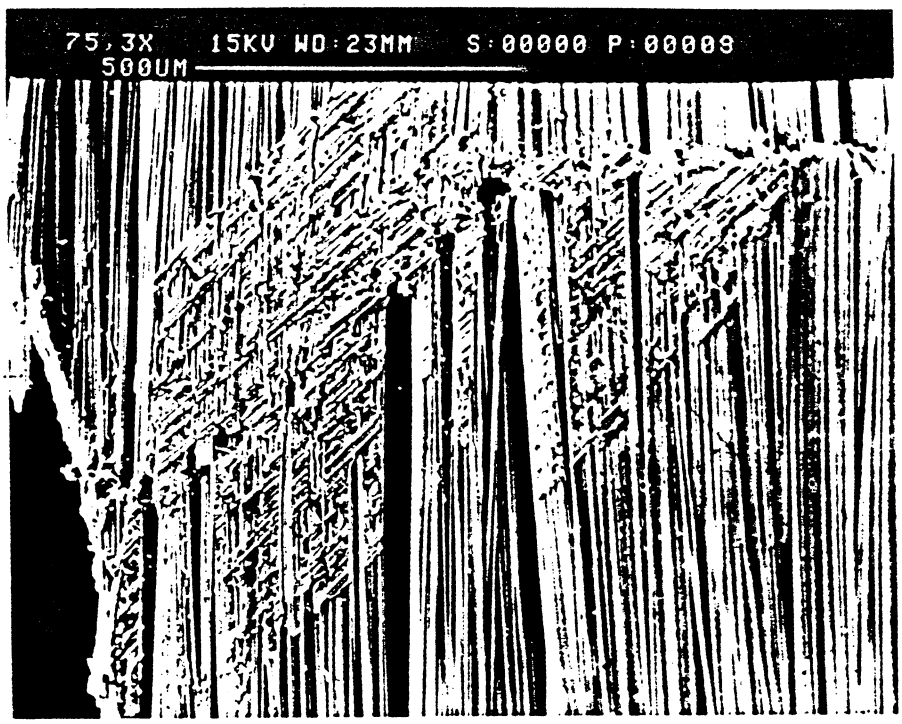


Fig.9. a) Fibre microbuckling failure in a 0-deg ply. The line of fracture is initially at 45-deg to the loading axis. Applied strain 0.52%.

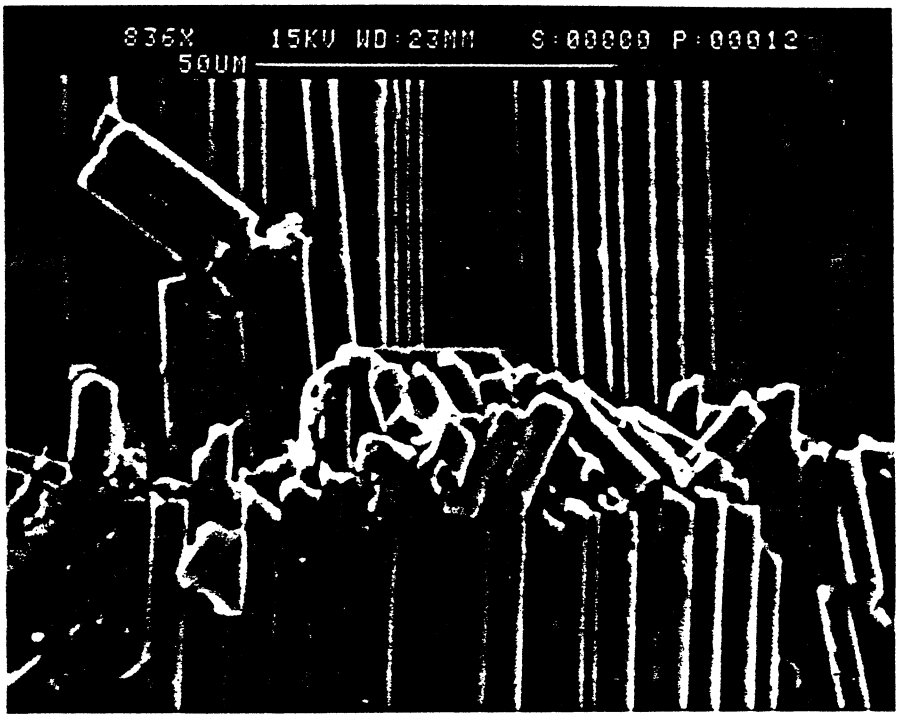


b) Magnification of (a), showing 0-deg buckled fibres.

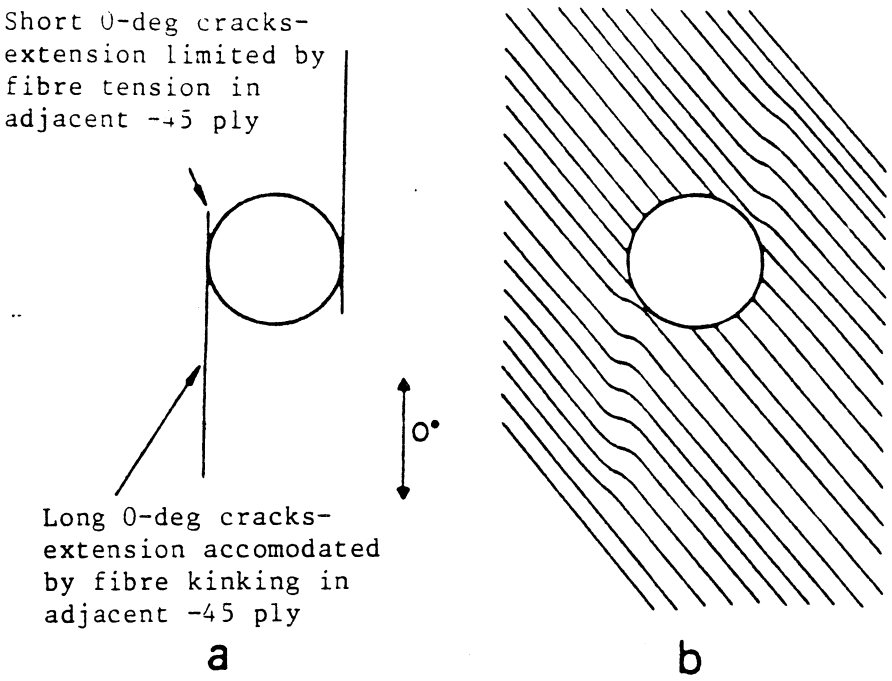


Fig.8. Asymmetric damage in central 0-deg plies and adjacent -45-deg plies showing: a) asymmetric longitudinal cracks in 0-deg plies; and b) Kinking of indivitual fibres in -45-deg plies [3].

b) SEM photograph illustrating fibre breakage in the -45-deg ply.

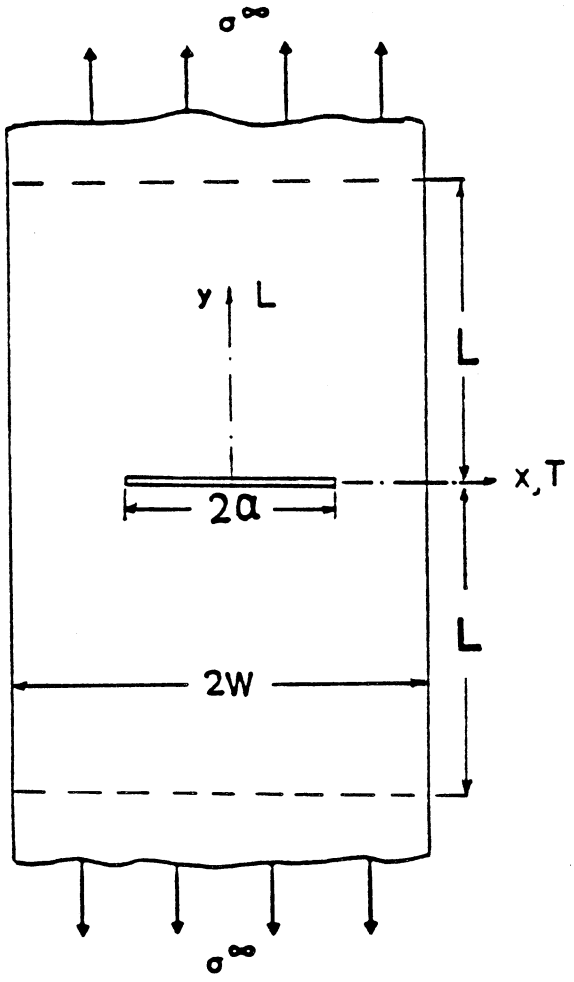


Fig.10. Geometry of centre-cracked test specimen.

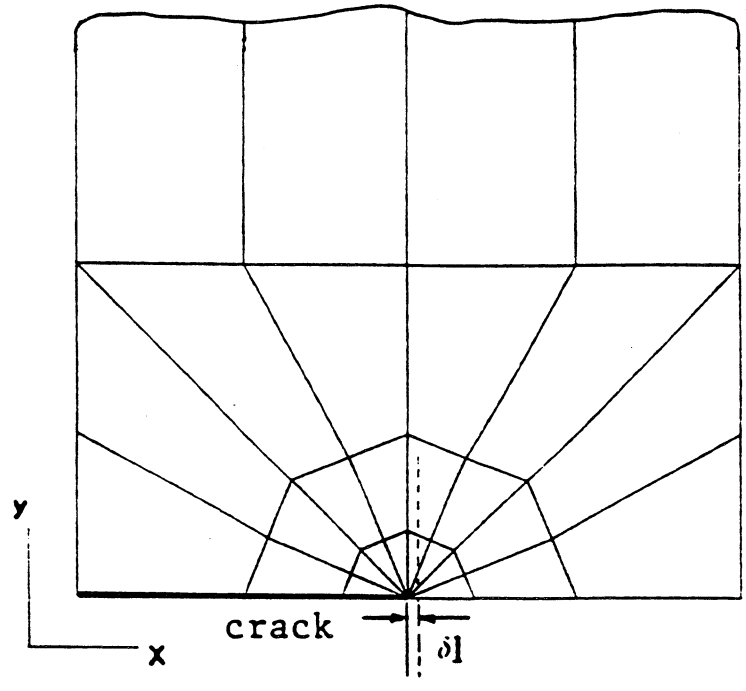


Fig.11. Finite element mesh for crack analysis. dl is the crack extension in the direction of crack advance.

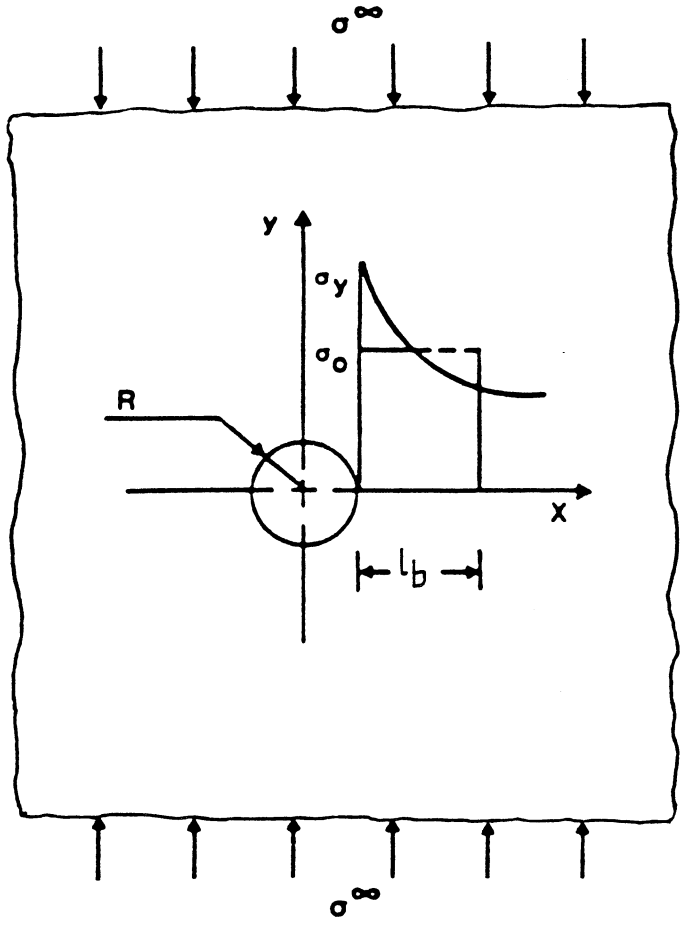


Fig.12. a) Stable growth of fibre-microbuckling.

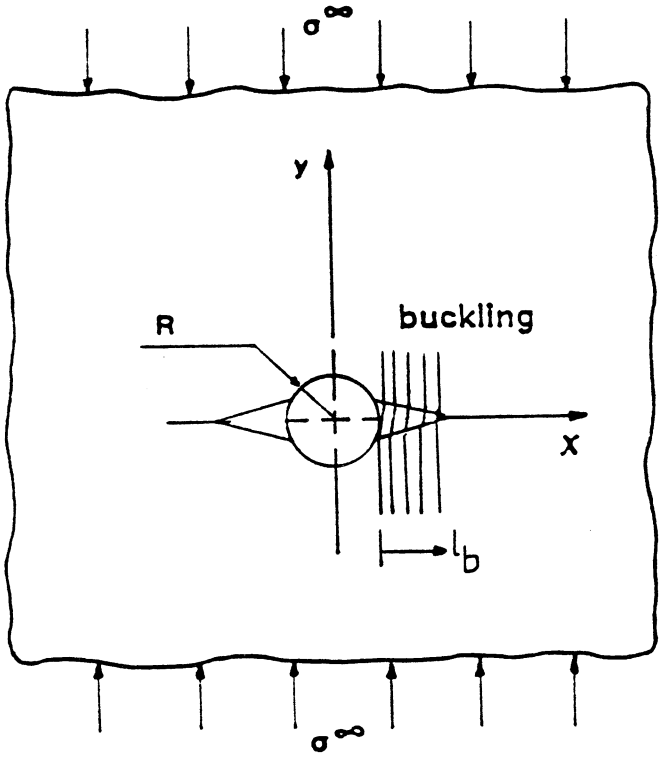


b) Unstable growth of fibre buckling, $K_I = K_{IC}$

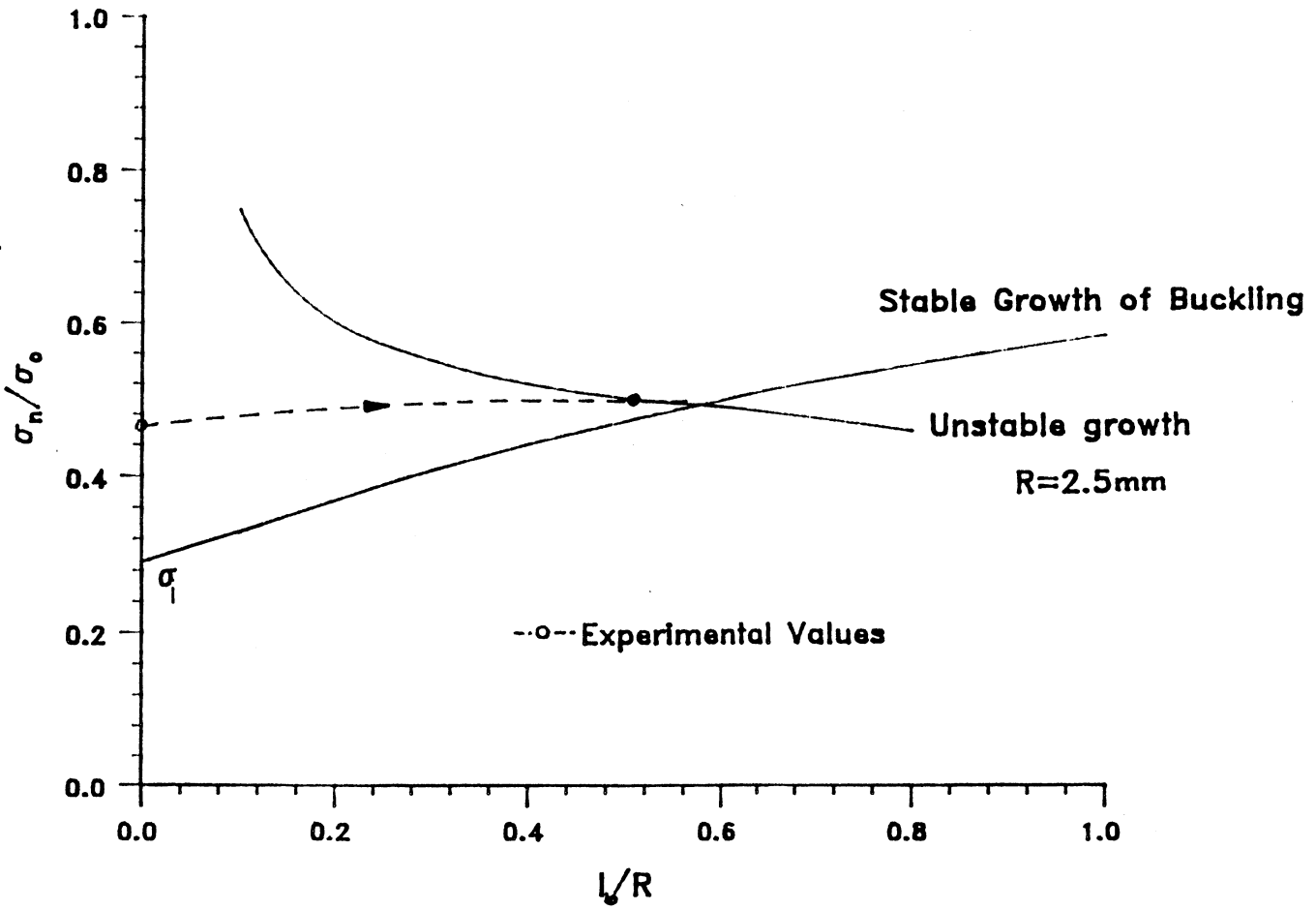


Fig.13. Strength prediction of an orthotropic plate with circular hole (d/W=0.1).